MIDDLE POMERANIAN SCIENTIFIC SOCIETY OF THE ENVIRONMENT PROTECTION
ŚRODKOWO-POMORSKIE TOWARZYSTWO NAUKOWE OCHRONY ŚRODOWISKA

Annual Set The Environment Protection
Rocznik Ochrona Środowiska

Volume/Tom 20. Year/Rok 2018 ISSN 1506-218X 221-240

Experimental Study of Air Lift Pump Delivery Rate

Marek Kalenik, Marek Chalecki
Warsaw University of Life Sciences – SGGW

1. Introduction

An air lift pump does not have any movable parts and it is used to lift liquids or liquid-solid mixes. The device is built of a vertical pipe, partly submerged in liquid, where air under pressure is introduced into its lower part. During introduction of air, a two-phase (liquid-air) or three-phase (liquid-air-solid) mix arises inside the vertical pipe, having lower density than the liquid. As the mix within the vertical pipe becomes lighter than the surrounding liquid, the mix is pushed up by the air.

Air lift pumps were usually used to transport liquid both in water supply and sewage systems. Nowadays in Poland, these devices are used to lift sewage and sewage sediments in small near-home container sewage-treatment plants and big group sewage-treatment plants (Sawicki 2004, Skoczko et al. 2016, Skoczko et al. 2017) as well as in high-rate filters with self-regenerating bed (Kalenik 2017) or for renovation of bored wells (Solecki 2010). However, in other countries, the air lift pumps have much wider application. They are used to aerate and mix water as well as to remove carbon dioxide from water in industrial fish farming (Barrut et al. 2012), to mix water in deep lakes and to aerate it by means of transport of water from the lake bed onto its surface (Fan et al. 2013). Due to the simple construction and high reliability of the air lift pumps, they are applied in various branches of industry, especially in the petrochemical industry to raise oil from dead wells (Hanafizadeh et al. 2011), in the chemical industry to transport corrosive, radioactive, arid or toxic fluids as well as to pump boiling fluids, where the change of liquid phase into gas phase occurs (Kassab et al. 2007). They are also used to

transport suspensions in mining industry and to lift manganese concretions from deep seabed up to ca. 4000-6000 m (Kassab et al. 2007).

A two-phase (liquid-gas) or three-phase (liquid-gas-solid) flow exists in the air lift pumps which is very difficult for mathematical modeling, for it depends on many factors and variables (Fujimoto et al. 2004, Kalenik 2017). The hydraulic operating conditions of two- and three-phase flow in the air lift pumps are very poorly identified. Some attempts are made to describe flow structures, occurring in various conditions of liquid-gas flow or liquid-gas-solid flow, and to work out so-called flow structure maps for them and mathematical models for simulation of flows occurring in the air lift pumps (Meng et al. 2013, Kim et al. 2014, Wahba et al. 2014).

Tests of air lift pumps built of rectangular (Esen 2010) and curved (Fujimoto et al. 2004) pipes were also carried out. The performed investigations of the air lift pumps with the curved pipes behind the air injector show that the pumping efficiency for solid bodies significantly falls in such air lift pumps. However, if only liquid is being pumped then the air lift pump pipe curvature does not affect its efficiency (Mahrous 2013). The performed investigations show that the air lift pumps are characterized by small working efficiency compared to conventional pumps (Tighzert et al. 2013, Kassab et al. 2009, Kalenik 2015, Kalenik & Malarski 2018).

There is no information in the technical and scientific literature on principles of calculations of flow rate of sand (Q_s) and water (Q_w) in air lift pumps used for lifting of filter bed (sand) in water conditioning filters with self-regenerating bed. Such types of air lift pumps are characterized by three-phase flow (water-sand-air). Moreover, there is no information how to design injectors to obtain the best operating parameters of the air lift pump. From the investigations to date it arises that the type of an injector and the diameter of a vertical pipe applied in the air lift pump affect its efficiency and hydraulic operating conditions (Fan et al. 2013, Kalenik 2017). The number, diameter and distribution of holes in the injector has very big influence on the types of structure of two-phase flow of air and liquid in air lift pumps. The types of the two-phase flow structures in the air lift pumps depend mainly on the air flow rate. Along with the rise in the air flow rate, the two-phase flow structures change in the air lift pumps. Other researchers also confirm that such dependences

occur in the air lift pumps (Hanafizadeh et al. 2011, Kalenik 2015). As the air flow rate grows in the air lift pumps, there become to occur: bubbly flow, slug flow, churn flow, annular flow. The researchers concluded that the slug flow is the most appropriate for air lift pumps for liquids (Hanafizadeh et al. 2011).

This paper presents the analysis of results of investigations of flow rate of an air lift pump which transports sand and water. The scope of the investigations encompassed the derivation of formulas for calculation of flow rate of sand (Q_s) and water (Q_w) in the PVC air lift pump with the internal diameter of the discharge pipe d = 0.03 m, by the fixed sand-water mix delivery head H: 0.40 m, 0.80 m, 1.20 m.

2. Methodology of derivation of the structural equation

Taking into consideration that the flow structures of air-water mix are so diverse and the work of air lift pumps is very dynamic and various (Kassab et al. 2009, Hanafizadeh et al. 2011, Kalenik 2015, Kalenik 2017), it must be stated that it is very hard to work out a classical mathematical model for derivation of a formula for calculation of a flow rate of sand and water in an air lift pump. Due to this, the dimensional analysis (Kokar 1979, Kalenik 2015, Kalenik 2017) was applied to determine the formula. Basing on the performed literature review and on the measurements made on the air lift pump test rig (Figure 1), an assumption was made that the air lift pump flow rate depends on the following dimensional variables: H – sand-water mix delivery head [m], Q_s – sand flow rate [$m^3 \cdot s^{-1}$], Q_w – water flow rate [$m^3 \cdot s^{-1}$], k – absolute roughness coefficient [m], p_b – barometric pressure [$kg \cdot m^{-1} \cdot s^{-2}$], p_a – air pressure [$kg \cdot m^{-1} \cdot s^{-2}$], d – discharge pipe diameter [m], Q_a – air flow rate [$m^3 \cdot s^{-1}$], ρ_w – water density [$kg \cdot m^{-3}$], ρ_a – air density [$kg \cdot m^{-3}$], ρ_s – wet sand density [$kg \cdot m^{-3}$], μ_w – water dynamic viscosity [$kg \cdot m^{-1} \cdot s^{-1}$], μ_a – air dynamic viscosity [$kg \cdot m^{-1} \cdot s^{-1}$], g – gravitational acceleration [$m \cdot s^{-2}$].

The absolute roughness coefficient k, which is equal 0.02 mm for PVC pipes, was also taken into consideration. However, the hydraulic resistance along the discharge pipe length was neglected because – as it results from the literature (Mahrous 2013, Tighzert et al. 2013, Wahba et al. 2014) – it is very low (unmeasurable), thus it must not be considered in calculations. In technical conditions, the vertical pipes in air lift pumps

are applied without thermal insulation, so the temperature of gas (air), liquid (water) and solids (sand) is close to the ambient temperature. Therefore it can be assumed that the temperature of gases, liquids and solids is constant along the vertical pipe and the flow of gases, liquids and solids is isothermal, thus p_a/ρ_a = const., p_a/ρ_w = const. and p_a/ρ_s = const. Along with the rise in delivery head (H) the flow of sand (Q_s) and water (Q_w) diminishes. Taking the above assumptions into account, the dimensional equation which describes the phenomenon being considered can be written in a form:

$$f\left(\frac{Q_s}{Hk},\frac{Q_w}{Hk},p_b,\frac{p_a}{\rho_w},\frac{p_a}{\rho_a},\frac{p_a}{\rho_s}\mu_w,\mu_a,d,Q_a,g\right)=0 \tag{1}$$

There is $n = 11$ dimensional quantities in this equation and their dimensions contain $i = 3$ basic units: m, kg, s. According to the Buckingham's Π-theorem, this equation can be transformed to a dependence of $n - i = 8$ mutually independent dimensionless parameters π. Three quantities were chosen: μ_a, d, Q_a, which contain the aforementioned basic units; their dimensional independence was checked below:

$$[\mathrm{kg}\cdot\mathrm{m}^{-1}\cdot\mathrm{s}^{-1}]^{a1}\cdot[\mathrm{m}]^{a2}\cdot[\mathrm{m}^3\cdot\mathrm{s}^{-1}]^{a3}=\mathrm{b},$$
$$\mathrm{kg}^{a1}\cdot\mathrm{m}^{-a1}\cdot\mathrm{s}^{-a1}\cdot\mathrm{m}^{a2}\cdot\mathrm{m}^{3a3}\cdot\mathrm{s}^{-a3}=\mathrm{b},$$
$$\mathrm{m}^{-a1+a2+3a3}\cdot\mathrm{kg}^{a1\cdot s-a1-a3}=[\mathrm{m}]^0\cdot[\mathrm{kg}]^0\cdot[\mathrm{s}]^0,$$
$$-a_1+a_2+3a_3=0\Rightarrow a_2=0,$$
$$a_1=0\Rightarrow a_1=0,$$
$$-a_1-a_3=0\Rightarrow a_3=0,$$

thus $a^1 = a^2 = a^3 = 0$, b = 1 (they are dimensionally independent).

The subsequent connection of the remaining five dimensional quantities with the product of the powers of the chosen dimensionally independent quantities allows to determine the dimensionless parameters π:

$$\pi_1=\frac{Q_s}{Hk}\mu_a^{a1}d^{a2}Q_a^{a3} \tag{2}$$

$$\pi_2=\frac{Q_w}{Hk}\mu_a^{b1}d^{b2}Q_a^{b3} \tag{3}$$

$$\pi_3=p_b,\mu_a^{c1}d^{c2}Q_a^{c3} \tag{4}$$

$$\pi_4 = \frac{p_a}{\rho_w} \mu_a^{d1} d^{d2} Q_a^{d3} \tag{5}$$

$$\pi_5 = \frac{p_a}{\rho_a} \mu_a^{e1} d^{e2} Q_a^{e3} \tag{6}$$

$$\pi_6 = \frac{p_a}{\rho_s} \mu_a^{f1} d^{f2} Q_a^{f3} \tag{7}$$

$$\pi_7 = \mu_w \mu_a^{g1} d^{g2} Q_a^{g3} \tag{8}$$

$$\pi_8 = g \mu_a^{h1} d^{h2} Q_a^{h3} \tag{9}$$

The substitution of these individual quantities and comparison of the power exponents standing by the basic units of the both sides of the subsequent equations (analogically as during checking of the dimensional independence of the quantities) yields the values of these quantities:

$$\pi_1 = \frac{Q_s d^2}{Hk Q_a} \tag{10}$$

$$\pi_2 = \frac{Q_w d^2}{Hk Q_a} \tag{11}$$

$$\pi_3 = \frac{p_b d^3}{\mu_a Q_a} \tag{12}$$

$$\pi_4 = \frac{p_a d^4}{\rho_w Q_a^2} \tag{13}$$

$$\pi_5 = \frac{p_a d^4}{\rho_a Q_a^2} \tag{14}$$

$$\pi_6 = \frac{p_a d^4}{\rho_s Q_a^2} \tag{15}$$

$$\pi_7 = \frac{\mu_w}{\mu_a} \tag{16}$$

$$\pi_8 = \frac{g d^5}{Q_a^2} \tag{17}$$

According to the Buckingham's Π-theorem, the dimensional equation (1) can be written in a form of dimensionless dependence between the parameters π:

$$f(\pi_1, \pi_2, \pi_3, \pi_4, \pi_5, \pi_6, \pi_7, \pi_8) = 0 \tag{18}$$

hence for:

- sand flow rate:

$$\pi_1 = f(\pi_2, \pi_3, \pi_4, \pi_5, \pi_6, \pi_7, \pi_8) \tag{19}$$

- water flow rate:

$$\pi_2 = f(\pi_1, \pi_3, \pi_4, \pi_5, \pi_6, \pi_7, \pi_8) \tag{20}$$

Substitution of the terms (10)-(17) instead of π, after rearrangement, gives the structural equation for:

- sand flow rate:

$$Q_s = f\left(\frac{Q_w d^2}{Hk Q_a}, \frac{p_b d^3}{\mu_a Q_a}, \frac{p_a d^4}{\rho_w Q_a^2}, \frac{p_a d^4}{\rho_a Q_a^2}, \frac{p_a d^4}{\rho_s Q_a^2}, \frac{\mu_w}{\mu_a}, \frac{g d^5}{Q_a^2}\right) \frac{Hk Q_a}{d^2} \tag{21}$$

- water flow rate:

$$Q_w = f\left(\frac{Q_s d^2}{Hk Q_a}, \frac{p_b d^3}{\mu_a Q_a}, \frac{p_a d^4}{\rho_w Q_a^2}, \frac{p_a d^4}{\rho_a Q_a^2}, \frac{p_a d^4}{\rho_s Q_a^2}, \frac{\mu_w}{\mu_a}, \frac{g d^5}{Q_a^2}\right) \frac{Hk Q_a}{d^2} \tag{22}$$

As the structural equations had been derived, an experiment was carried out to determine their numerical coefficients.

In Eqs. (21), (22), the dimensional quantities:

- ρ_w, μ_w – describe physical features of water,
- ρ_a, μ_a – describe physical features of air,
- ρs – describes physical features of sand,
- d, k, H – characterize the research object, i.e. discharge pipe – they have constant values,
- p_a, Q_a – describe so-called input quantities being a result of intentional actions being applied on the object being examined – they are controlled and controllable quantities,
- Q_s, Q_w – describe so-called output quantities – they are a response of

the object being examined on the input quantities (actions).

On the other hand, the dimensionless quantity in Eqs. (21) and (22) describes:

- π_1 – ratio of forces evoked by the sand flow to friction forces,
- π_2 – ratio of forces evoked by the water flow to friction forces,
- π_3 – ratio of forces evoked by the barometric pressure to friction forces,
- π_4, π_5, π_6 – ratio of forces evoked by the air pressure to dynamic forces,
- π_7 – ratio of water viscosity (friction) forces to air viscosity (friction) forces,
- π_8 – ratio of gravity forces to dynamic forces evoked by the air flow.

3. Experimental procedures

3.1. Description of the air lift pump test rig

Figure 1 shows the construction and operating principle of a stand for investigations of hydraulic operating conditions of air lift pumps (air lift pump test rig). After the opening of a ball valve (2), a pipeline (1) delivered water to a tank (3), filled with sand. During the tests the tank (3) was permanently filled with water up to the height of 1.0 m. After the opening of another ball valve (9), the excess of the water being delivered to the tank (3) was carried by an overfall (8) to the sewerage through a floor inlet (13). A draining pipeline (16) served to empty the tank (3) from water after the ball valve (15) opening. Inside of the tank (3), at the height of 0.20 m upon its bottom, a PVC discharge pipe (5) with the internal diameter of 0.03 m was mounted. The measurements of the air lift pump delivery rate were carried out for the three sand-water mix delivery heads (H): 0.40 m, 0.80 m, 1.2 m, measured over the water level in the tank (3). In the discharge pipe (5), at the height of 0.30 m over its lower edge, an air injector (10) was mounted. To measure water temperature in the tank (3), an electronic resistance thermometer (19) was applied.

Figure 2 shows a constructive solution of the tested air injector which provided a one-point air supply to the air lift pump. The injector had a form of a steel, externally screwed tip (2) with the internal diameter of 0.01 m. The steel tip (2) had an elastic pipe (7, Figure 1) put on it, having the external diameter of 0.013 m and supplying air from a compressor

(25) to the injector (10). At the air supplying pipe (7) an electromagnetic air flow meter (20), piezoelectric pressure sensor (21), electronic resistance thermometer (22) to measure air temperature as well as a poppet valve (23) and ball cut-off valve (24) were mounted.

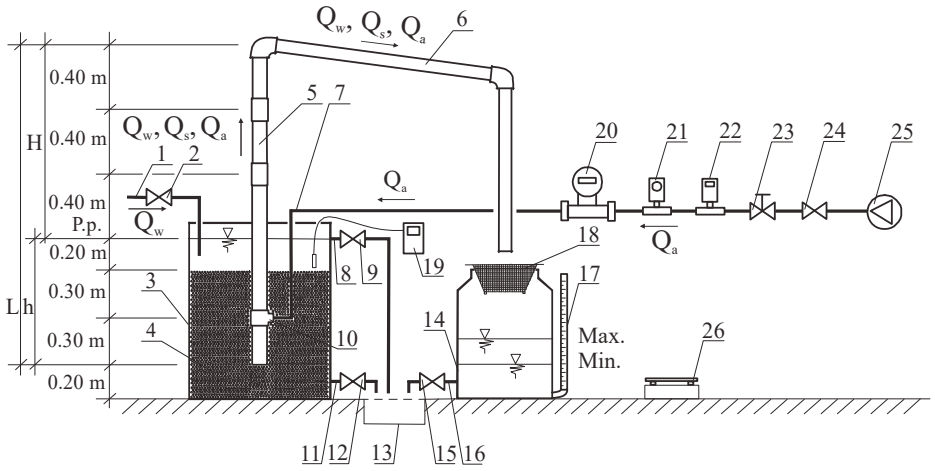

Fig. 1. Scheme of the air lift pump test rig: 1 – discharge pipe, 2, 9, 12, 15, 24 – ball cut-off valve, 3 – tank with water and sand, 4 – sand, 5 – discharge pipe d = 0.03 m, 6 – water, sand and air channeling pipe, 7 – air supplying pipe, 8 – overfall, 10 – air injector, 11, 16 – draining pipe, 13 – floor inlet, 14 – measuring container, 17 – scaled water level gauge, 18 – basket, 19, 22 – electronic resistance thermometer, 20 – electromagnetic air flow meter, 21 – piezoelectric pressure sensor, 23 – poppet valve, 25 – compressor, 26 – scales, h – discharge pipe submergence length, L – discharge pipe length-to-outlet, H – water-sand mix delivery head

Rys. 1. Schemat stanowiska do badania powietrznego podnośnika: 1 – rurociąg doprowadzający wodę, 2, 9, 12, 15, 24 – odcinający zawór kulowy, 3 – zbiornik z wodą i piaskiem, 4 – piasek, 5 – rurociąg tłoczny d = 0,03 m, 6 – rurociąg odprowadzający wodę, piasek i powietrze, 7 – rurociąg doprowadzający powietrze, 8 – przelew, 10 – mieszacz, 11, 16 – rurociąg spustowy, 13 – wpust podłogowy, 14 – zbiornik pomiarowy, 17 – wodowskaz ze skalą, 18 – koszyk, 19, 22 – elektroniczny termometr, 20 – elektroniczny przepływomierz powietrza, 21 – elektroniczny czujnik ciśnienia, 23 – zawór grzybkowy, 25 – sprężarka, 26 – waga, h – długość zanurzenia rurociągu tłocznego, L – długość rurociągu tłocznego do wylotu, H – wysokość podnoszenia mieszaniny piasku i wody

The investigations were performed with use of Endress & Hauser devices. The electromagnetic air flow meter (20) measuring range was 0.0 to 30.0 $m^3 \cdot h^{-1}$ and the piezoelectric pressure sensor (20) measuring range – 0.0 to 400 kPa. According to the Endress & Hauser catalogue, the measuring error of the applied electromagnetic air flow meter and piezoelectric pressure sensor is lower than 1% and the output current signal falls into the range 4-20 mA. The measuring accuracy of the applied thermometer, however, was ±1°C and its measuring resolution 0.1°C.

The measurements concerned water and air temperature, air pressure, barometric pressure, air flow rate, water volume and air lift pump operating time. The scale (26) weighted the sand. The poppet valve (23) was used to regulate the air pressure.

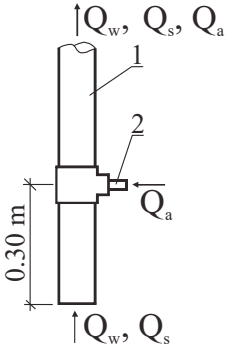

Fig. 2. Construction of the air injector: 1 – discharge pipe d = 0.03 m, 2 – steel tip to join an air supplying pipe
Rys. 2. Konstrukcja mieszacza: 1 – rurociąg tłoczny d = 0,03 m, 2 – stalowa końcówka do podłączenia rurociągu doprowadzającego powietrze

To measure the air lift pump delivery rate, the measuring vessel method was applied, i.e. there was used a plastic measuring container (14) which was scaled at each 1 dm^3. The measuring container (14) capacity scale was put on the transparent water-level gauge (17), mounted at the side of the measuring container (14). Such solution allowed to read very precisely the volume of the water lifted by the air lift pump per time unit. For a fixed delivery head (H), the lifted water-sand mix flew down through the channeling pipe (6) with the internal diameter 0.03 m to a basket (18) placed in the inlet to the measuring container (14). During the measurements the sand was collected in the basket (18) and the water from the

basket (18) flew down into the measuring container (14). The wet sand collected in the basket was weighted. The sand applied in the tests had graining 0.8-2.0 mm and the density in wet condition $\rho_s = 1632.0$ kg·m^{-3}.

3.2. Methodology of investigations of the air lift pumps

Before each measuring series had begun on the air lift pump test rig (Figure 1), an actual barometric pressure (p_b) was measured using the piezoelectric pressure sensor (21). Then, on the water-level gauge (17) connected to the measuring container (14), it was marked the minimum level of a water free surface in the measuring container (14) by which the stop-watch was switched on as well as the maximum level of free surface of water by which the stop-watch was switched off. The level marked on the water-level gauge (17) scale referred to a certain water volume (V_w).

The measurement of the sand flow rate (Q_s) and water flow rate (Q_w) was started from the opening of the valves (2, 9), filling the tank (3) with sand (4) and water, turning on the compressor (25) and opening the valve (24) on the pipeline (7) supplying the air injector (10) with air. Then a demanded value of the air pressure (p_a) was fixed on the piezoelectric pressure sensor (21) using the poppet valve (23). As the determined air pressure had been fixed, some quantity of sand and water – depending on the air lift pump flow rate – flew out from the tank (3). To make the measurement reliable, the water level in the tank (3) had to be kept constant. Changes of the submergence of the air injector (10) or the water level changes in the tank (3) cause significant changes in the air lift pump flow rate. The constant water level in the tank (3) was kept using the valve (2) placed on the discharge pipe (1) supplying water to the tank (3). Each time the valve (2) was set in the position which balanced the water flux through the channeling pipe (6) for a given value of the air pressure. The observations and regulations of the water level in the tank (3) were performed relatively to the level in the overfall (8) which channeled the water excess. As these actions were completed and the working conditions of the air lift pump stabilized, the measurement started. At first, for a fixed value of the air pressure, the air flow rate (Q_a) was being read from the electromagnetic air flow meter (20) and the air and water temperatures – from the electronic resistance thermometers (19 – water, 22 – air). As the water-level gauge (17) showed that the water free surface in the measuring container (14) reached the marked minimum level,

then the stop-watch was switched on and the basket (18) was placed under the water, air and sand channeling pipe (6), in the inlet to the measuring container (14). The stop-watch measured a container (14) filling time (t) till the moment when the water free surface reached the marked maximum level – then the stop-watch was switched off and the poppet valve (23), cutting off the air to the air injector (10), was turned off. During the measurement the sand gathered in the basket (18) and the water from the basket flew down to the measuring container (14). As the measuring container (14) filling time t was read, the sand in the basket (18) was weighted with the scale (26) and then the sand was dropped into the basket again. Then the measuring container (14) was emptied, a next value of the air pressure was set on the piezoelectric pressure sensor (21) and a next measurement started. The measurements were carried out for the fixed air pressure (p_a) from 110 till 180 kPa with intervals 5 kPa. The water flow rate (Q_w) was calculated by dividing the volume (V_w) of water being in the measuring container (14) through the filling time (t) and the sand flow rate (Q_s) was calculated by dividing the weight (C_s) of the sand collected in the basket (18) through the filling time (t) and the density (ρ_s) of the wet sand. During the tests, five measuring series were carried out – each of them for a fixed value of the air pressure (pa) and all three sand-water mix delivery heads (H): 0.40 m, 0.80 m, 1.20 m, measured relatively to the water free surface in the tank (3).

4. Results of the tests and their discussion

Figure 3 presents a dependence of the air flow rate (Q_a) in the air lift pump vs. the air pressure (pa) and sand-water mix delivery head (H). Analysis of the obtained results allows to state that the air flow rate in the air lift pump rises along with the air pressure. On the other hand, the rise in the sand-water mix delivery head by the constant submergence of the air injector and big values of the air pressure slightly affected the fall of the air flow rate. Independently on the sand-water mix delivery head, the values of the air flow rate by a given air pressure were comparable, what resulted from big quantity of air.

Figures 4 and 5 present the results of measurements (solid lines) of sand flow rate (Q_s) and water flow rate (Q_w) depending on the air pressure (p_a) and water-sand mix delivery head (H) as well as the results of

calculations (broken lines) performed with use of the determined formulas (23, 24). In the tested air lift pump, for the given water-sand mix delivery heads, the values of water flow rate are higher than those of the sand flow rate. The values of water and sand flow rate fall along with the rise in the water-sand mix delivery head and initially grow with the rise of air pressure, achieve the maximum and then they fall.

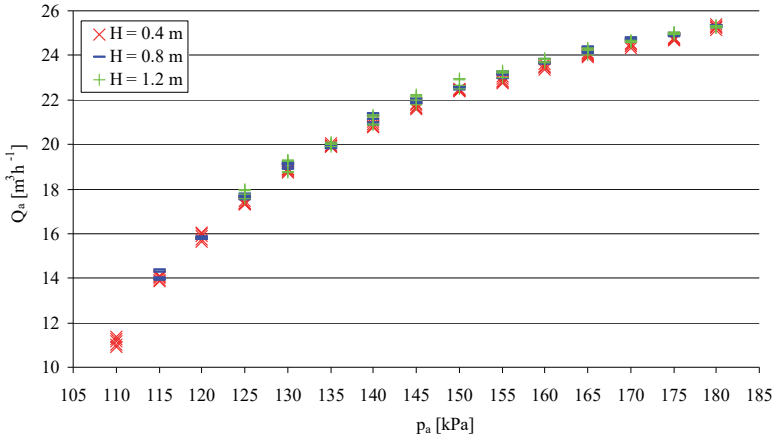

Fig. 3. Air flow rate (Q_a) in the air lift pump vs. air pressure (p_a) and sand-water mix delivery head (H)
Rys. 3. Zależność natężenia przepływu powietrza (Q_a) w podnośniku powietrznym od ciśnienia powietrza (p_a) i wysokości podnoszenia mieszaniny piasku i wody (H)

To enable the outflow of the sand of graining 0.8-2.0 mm from the air lift pump on a demanded delivery head, it must be provided an appropriate minimum air pressure which forces an appropriate air flow rate in the discharge pipe. Along with the rise in the water-sand mix delivery head the minimum demanded air pressure grew, thus so did the minimum air flow rate in the discharge pipe. In the tested air lift pump, for the water-sand mix delivery head 0.40 m, the demanded minimum air pressure was equal 110 kPa what corresponded to the average minimum air flow rate 11.6 $m^3 \cdot h^{-1}$. For the water-sand mix delivery heads equal 0.8 m and 1.2 m these values were equal 115 kPa and 14.10 $m^3 \cdot h^{-1}$ as well as 125 kPa and 17,85 $m^3 \cdot h^{-1}$, respectively.

For the given water-sand mix delivery heads, when the air pressure exceeded 150 kPa, what corresponds to the average air flow rate 22.59 $m^3 \cdot h^{-1}$, the values of sand and water flow rates did not grow further but started to reduce. This phenomenon is described in the literature (Hanafizadeh et al. 2011, Meng et al. 2013, Kalenik 2017, Kalenik & Malarski 2018). Due to this fact, the maximum demanded air pressure for the tested air lift pump with the applied (Figure 2) air injector should not exceed 150 kPa.

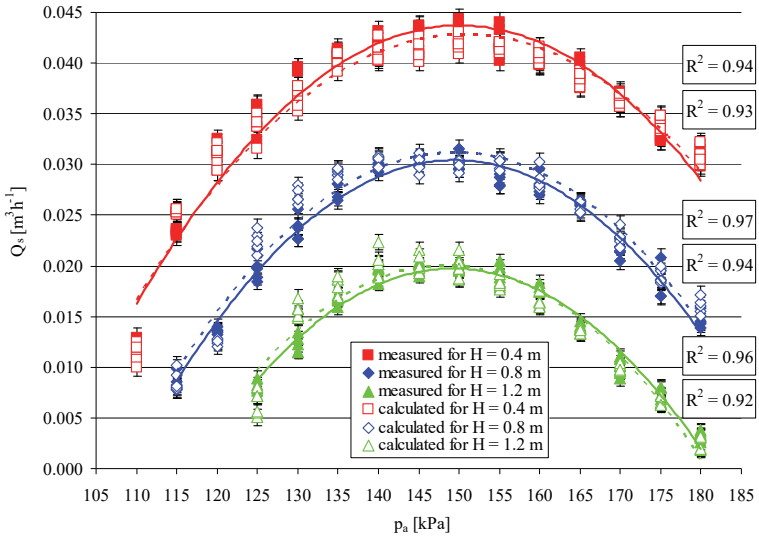

Fig. 4. Sand flow rate (Q_s) vs. air pressure (p_a) according the measurements and calculations

Rys. 4. Zależność natężenia przepływu piasku (Q_s) od ciśnienia powietrza (p_a) według pomiarów i obliczeń

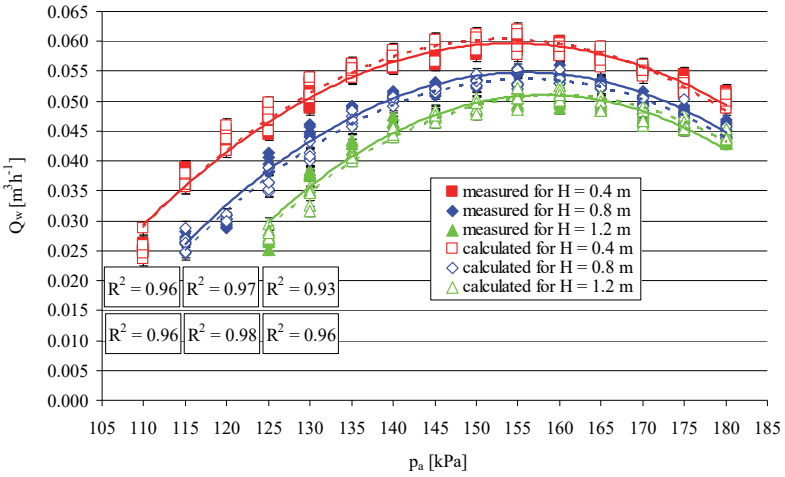

Fig. 5. Water flow rate (Q_w) vs. air pressure (p_a) according the measurements and calculations
Rys. 5. Zależność natężenia przepływu wody (Q_w) od ciśnienia powietrza (p_a) według pomiarów i obliczeń

To determine the flow capacity of the tested air lift pump, appropriate empirical formulas were derived. In this aim, using the measurements performed on the air lift pump test rig (Figures 1 and 2), the dimensionless parameters π_1 (10), π_2 (11), π_3 (12), π_4 (13), π_5 (14), π_6 (15), π_7 (16), π_8 (17) were calculated from the derived structural equations for Q_s (21) and Q_w (22). Basing on the measured temperatures of water and air, the following constants were calculated from the tables (Orzechowski et al. 2001): the density of water (ρ_w) and air (ρ_a), the dynamic viscosity of water (μ_w) and air (μ_a). Then appropriate data tables were built and – using the multiple regression method and the computer package STATISTICA – the numerical coefficients to the empirical formulas for calculation of Q_s and Q_w. Substitution of the determined numerical coefficients to the structural equations (21, 22) and reduction of significant digits in them for the sake of facilitation finally yields the following empirical formulas for calculation of sand and water flow rate in air lift pumps:

$$Q_s = \left(\begin{array}{l} -1.23 \cdot 10^{-1} + 8.36 \cdot 10^{-1} \dfrac{Q_w d^2}{Hk Q_a} + 5.39 \cdot 10^{-9} \dfrac{p_b d^3}{\mu_a Q_a} - 3.4 \cdot 10^{-2} \dfrac{p_a d^4}{\rho_w Q_a^2} \\ -1.236 \cdot 10^{-5} \dfrac{p_a d^4}{\rho_a Q_a^2} - 2.7 \cdot 10^{-2} \dfrac{p_a d^4}{\rho_s Q_a^2} + 1.17 \cdot 10^{-3} \dfrac{\mu_w}{\mu_a} + 9.29 \dfrac{g d^5}{Q_a^2} \end{array} \right) \frac{Hk Q_a}{d^2} \quad (23)$$

$$Q_w = \left(\begin{array}{l} 1.21 \cdot 10^{-1} + 1.19 \dfrac{Q_s d^2}{Hk Q_a} - 6.23 \cdot 10^{-9} \dfrac{p_b d^3}{\mu_a Q_a} + 3.95 \cdot 10^{-2} \dfrac{p_a d^4}{\rho_w Q_a^2} \\ +2.04 \cdot 10^{-5} \dfrac{p_a d^4}{\rho_a Q_a^2} + 3.56 \cdot 10^{-2} \dfrac{p_a d^4}{\rho_s Q_a^2} - 1.07 \cdot 10^{-3} \dfrac{\mu_w}{\mu_a} - 13.32 \dfrac{g d^5}{Q_a^2} \end{array} \right) \frac{Hk Q_a}{d^2} \quad (24)$$

where:
Q_s – sand flow rate [$m^3 \cdot s^{-1}$],
Q_w – water flow rate [$m^3 \cdot s^{-1}$],
p_b – barometric pressure [$kg \cdot m^{-1} \cdot s^{-2}$],
Q_a – air flow rate [$m^3 \cdot s^{-1}$],
H – sand-water mix delivery head [m],
k – absolute roughness coefficient [m],
p_a – air pressure [$kg \cdot m^{-1} \cdot s^{-2}$],
d – discharge pipe diameter [m],
ρ_w – water density [$kg \cdot m^{-3}$],
ρ_a – air density [$kg \cdot m^{-3}$],
ρ_s – wet sand density [$kg \cdot m^{-3}$],
μ_w – water dynamic viscosity [$kg \cdot m^{-1} \cdot s^{-1}$],
μ_a – air dynamic viscosity [$kg \cdot m^{-1} \cdot s^{-1}$],
g – gravitational acceleration [$m \cdot s^{-2}$].

The functional dependence between the flow rates of sand (Figure 4) and water rate (Figure 5) on the one hand and the air pressure on the other hand presents a nonlinear trend in the whole range of the values of p_a – both for the values of Q_s and Q_w obtained from the measurements and from the formulas (23), (24). The deviations of Q_s and Q_w obtained from the calculations related to those obtained from the measurements were small for the water-sand mix delivery heads being tested. The trend (regression) was of second degree in the whole range of the values of the air pressure for the values of Q_s and Q_w obtained from the measurements and calculations. The trend lines for the values of Q_s and Q_w obtained from the calculations were slightly shifted in relation to the values of Q_s

and Q_w obtained from the measurements. Figures 4 and 5 show also the pairs of coefficients of determination (R^2) from the sample. In Figure 4, the higher values of R^2 concern the measured values of Q_s and the lower ones – the values calculated from (23); whereas in Figure 5, the lower values of R^2 concern the measured values of Q_w and the higher ones – the values calculated from (24). The values of R^2 were higher than 0.92 what indicates that the water and sand flow rate in the air lift pump at least in 92% depended on the air pressure, thus on the air flow rate and the water-sand mix delivery head and only in 8% on remaining factors like the density of water, air and sand or the gravitational acceleration.

To evaluate the accuracy of the formulas (23), (24), the calculated values of Q_s and Q_w were compared to those measured on the test rig. It has been stated that within the following ranges of the values of the presented parameters: d = 0.03 m, 110 kPa ≤ p_a ≤ 180 kPa, $2.15 \cdot 10^{-3}$ $m^3 \cdot h^{-1}$ ≤ $Q_s \leq 4.23 \cdot 10^{-2}$ $m^3 \cdot h^{-1}$, $2.76 \cdot 10^{-3}$ $m^3 \cdot h^{-1} \leq Q_w \leq 6.27 \cdot 10^{-2}$ $m^3 \cdot h^{-1}$, 10.93 m^3·h-1 ≤ $Q_a \leq 25.39$ $m^3 \cdot h^{-1}$, 1.3330 $kg \cdot m^{-3} \leq \rho_a \leq 2.1836$ $kg \cdot m^{-3}$, 999.3336 $kg \cdot m^{-3}$ ≤ $\rho_w \leq 999.6184$ $kg \cdot m^{-3}$, ρ_s = 1632.0 [$kg \cdot m^{-3}$], $1.1796 \cdot 10^{-3}$ $kg \cdot m^{-1} \cdot s^{-1} \leq \mu_w \leq$ $1.2084 \cdot 10^{-3}$ $kg \cdot m^{-1} \cdot s^{-1}$, $1.7755 \cdot 10^{-5}$ $kg \cdot m^{-1} \cdot s^{-1} \leq \mu_a \leq 1.7855 \cdot 10^{-5}$ $kg \cdot m^{-1} \cdot s^{-1}$, an average deviation of Q_s does not exceed 4% for the water-sand mix delivery head of H = 0.40 m, 6% for H = 0.80 m and 10% for H = 1.20 m; whereas an average deviation of Q_w does not exceed 3% for the water-sand mix delivery head of H = 0.40 m and H = 0.80 m, 4% for H = 1.20 m. The dimensional analysis of the formulas (23), (24) proved that the dimensions of their both sides are consistent.

Furthermore, Figures 4 and 5 contain standard error bars which are small for the measured and calculated values of Q_s and Q_w. The standard error for the measured values oscillated between 0.7% and 8.1% (average 2.6%), whereas for the calculated values – between 0.6% and 12.7% (average 2.9%). The standard error was calculated with use of the STATISTICA computer program.

5. Conclusions

For the tested air lift pump, the air flow rate (Q_a) increased along with the increase of the air pressure (p_a). The flow rate of water (Q_w) and sand (Q_s) also increased along with the rise in the air pressure, then reached a maximum and felt. Along with the increase of the water-sand

mix delivery head (H), the flow rate of water and sand decreased and the values of the water flow rate (Q_w) were higher than those of the sand flow rate (Q_s).

For the tested air lift pump with the internal diameter of the discharge pipe 0.03 m with the applied air injector, the water and sand flow rates increased along with the rise in the air pressure within the range 110-150 kPa whereas they decreased for higher values of the air pressure. Due to this, it is recommended that the maximum air pressure for such devices should be higher than 110 kPa and should not exceed 150 kPa.

The values of the sand and water flow rates calculated from the derived formulas (23), (24) very well coincided with those determined from the direct measurements. Due to this, these formulas can be used for design of air lift pumps with the air injector presented in Figure 2.

References

Barrut, B., Blancheton, J-P., Champagne, J-Y., Grasmick, A. (2012). Mass transfer efficiency of a vacuum air lift – application to water recycling in aquaculture systems. *Aquacultural Engineering, 46*, 18-26.

Esen, I. I. (2010). Experimental investigation of a rectangular airlift pump. *Advances in Civil Engineering*, ID 789547, 5, doi:10.1155/2010/789547.

Fan, W., Chen, J., Pan, Y., Huang, H., Chen, C-T. A., Chen, Y. (2013). Experimental study on the performance of air-lift pump for artificial upwelling. *Ocean Engineering, 59*, 47-57.

Fujimoto, H., Murakami, S., Amura, A., Takuda, H. (2004). Effect of local pipe bends on pump performance of a small air-lift system in transporting solid particles. *International Journal of Heat and Fluid Flow, 25*, 996-1005.

Hanafizadeh, P., Ghanbarzadeh, S., Saidi, M. H. (2011). Visual technique for detection of gas–liquid two-phase flow regime in the air lift pump. *Journal of Petroleum Science and Engineering, 75*, 327-335.

Kalenik, M. (2015). Badania modelowe sprawności powietrznego podnośnika cieczy. *Ochrona Środowiska, 37(4)*, 39-46.

Kalenik, M. (2017). Badania modelowe strumienia objętości piasku i wody w podnośniku powietrznym. *Ochrona Środowiska, 39(1)*, 45-52.

Kalenik, M., Malarski, M. (2018). Badania wydajności powietrznego podnośnika wyposażonego w mieszacz z perforowaną gumową membraną. *Acta Scientiarum Polonorum. Formatio Circumiectus*, *17(1),* 21-31.

Kassab, S. Z., Kandil, H. A., Warda, H. A., Ahmedb, W. H. (2007). Experimental and analytical investigations of airlift pumps operating in three-phase flow. *Chemical Engineering Journal, 131*, 273-281.

Kassab, S. Z., Kandil, H. A., Warda, H. A., Ahmed, W. H. (2009). Air-lift pumps characteristics under two-phase flow conditions. *International Journal of Heat and Fluid Flow, 30*, 88-98.

Kim, S. H., Sohn, C. H., Hwang, J. Y. (2014). Effects of tube diameter and submergence ratio on bubble pattern and performance of air-lift pump. *International Journal Multiphase Flow, 58*, 195-204.

Kokar, M. (1979). Zarys procedury formułowania praw fizycznych w języku analizy wymiarowej. *Inżynieria Chemiczna*, *9(2)*, 361-369.

Mahrous, A.-F. (2013). Experimental study of airlift pump performance with s-shaped riser tube bend. *International Journal Engineering and Manufacturing, 1*, 1-12.

Meng, Q., Wang, C., Chen, Y., Chen, J. (2013). A simplified CFD model for air-lift artificial upwelling. *Ocean Engineering, 72*, 267-276.

Orzechowski, Z., Prywer, J., Zarzycki, R. (2001). *Zadania z mechaniki płynów w inżynierii środowiska*. Warszawa: Wydawnictwa Naukowo-Techniczne.

Sawicki, J.M. (2004). Aerated grit chambers hydraulic design equations. *Journal of Environmental Engineering*, *130(9)*, 1050–1058.

Skoczko, I., Ofman, P., Szatyłowicz, E. (2016). Zastosowanie sztucznych sieci neuronowych do modelowania procesu oczyszczania ścieków w małej oczyszczalni ścieków. *Rocznik Ochrona Środowiska, 18*, 493-506.

Skoczko, I., Struk-Sokołowska, J., Ofman, P. (2017). Modelowanie zmian parametrów ścieków oczyszczonych z wykorzystaniem sztucznych sieci neuronowych. *Rocznik Ochrona Środowiska, 19*, 633-650.

Solecki, T. (2010). Analiza i ocena możliwości renowacji odwiertu w uzdrowisku Połczyn. *Wiertnictwo Nafta Gaz, 27(3),* 617-627.

Tighzert, H., Brahimi, M., Kechroud, N., Benabbas, F. (2013). Effect of submergence ratio on the liquid phase velocity, efficiency and void fraction in an air-lift pump. *Journal of Petroleum Science and Engineering, 110*, 155-161.

Wahba, E.M., Gadalla, M.A., Abueidda, D., Dalaq, A., Hafiz, H., Elawadi, K., Issa, R. (2014). On the Performance of Air-Lift Pumps: from Analytical Models to Large Eddy Simulation. *Journal of Fluids Engineering, 136(11)*, 1-7.

Eksperymentalne badania wydajności powietrznego podnośnika

Streszczenie

W artykule przedstawiono analizę wyników badań natężenia przepływu piasku (Q_s) i wody (Q_w) w podnośniku powietrznym. Badania wykonywano na wybudowanym w laboratorium w skali 1:1 stanowisku do badania podnośnika

powietrznego. W artykule przedstawiono budowę i zasadę działania stanowiska badawczego oraz omówiono metodykę wyznaczenia empirycznych wzorów do obliczania natężenia przepływu piasku i wody. Przeprowadzono analizę porównawczą wartości natężenia przepływu piasku i wody wyznaczonych z bezpośrednich pomiarów z wartościami obliczonymi za pomocą wyznaczonych empirycznych wzorów. Zakres badań obejmował wyprowadzenie wzorów do obliczania natężenia przepływu piasku i wody w podnośniku powietrznym z tworzywa sztucznego PVC o średnicy wewnętrznej rurociągu tłocznego $d = 0{,}03$ m, przy zadanej wysokości podnoszenia mieszaniny piasku i wody H: 0,40 m, 0,80 m, 1,20 m. Do wyznaczenia empirycznych wzorów do obliczania natężenia przepływu piasku i wody zastosowano analizę wymiarową i metodę regresji wielokrotnej. W badanej konstrukcji podnośnika powietrznego wraz ze wzrostem wysokości podnoszenia mieszaniny piasku i wody, natężenie przepływu piasku i wody malało, a wartości natężenia przepływu wody były większe w stosunku do wartości natężenia przepływu piasku. W badanym urządzeniu ciśnienie powietrza nie może być mniejsze niż 110 kPa i nie powinno przekraczać 150 kPa, ponieważ przy wyższych ciśnieniach powietrza natężenie przepływu piasku i wody zaczynało spadać. Wartości natężenia przepływu piasku i wody obliczone za pomocą wyprowadzonych wzorów, bardzo dobrze pokrywały się z wartościami wyznaczonymi z bezpośrednich pomiarów.

Abstract

This paper presents analysis of results of investigations of flow rate of sand (Q_s) and water (Q_w) in an air lift pump. The investigations were performed on an air lift pump test rig, constructed in a laboratory on a scale of 1:1. The paper describes the construction and working principle of this air lift pump test rig and presents a methodology of derivation of empirical formulas for calculation of sand and water flow rate. A comparative analysis of the values of the sand and water flow rate obtained in direct measurements with analogical values of flow rate calculated with use of the derived empirical formulas was carried out. The research scope encompassed the derivation of the aforementioned empirical formulas in the PVC air lift pump with the internal diameter of the discharge pipe $d = 0.03$ m by the fixed sand-water mix delivery heads H: 0.40 m, 0.80 m, 1.20 m. To derive the empirical formulas for calculation of the sand and water flow rate, dimensional analysis and multiple regression was applied. In the air lift pump being tested, the water and sand flow rate felt along with the rise in the delivery head and the water flow rate was higher than the sand flow rate. Air pressure in such devices cannot be lower than 110 kPa and cannot exceed 150 kPa as for higher values of air pressure the sand and water flow rate starts to fall. The values of the sand and water flow rate calculated with use of

the derived formulas coincide very well with the values determined from the direct measurements.

Słowa kluczowe:
podnośnik powietrzny, mieszacz, przepływ trójfazowy, natężenie przepływu piasku, natężenie przepływu wody

Keywords:
air lift pump, air injector, three-phase flow, sand flow rate, water flow rate